RSC Advances

PAPER

View Article Online
View Journal | View Issue

Cite this: *RSC Adv.*, 2024, **14**, 24424

NIR light-triggered photodynamic antibacterial nanofiber membrane based on polycaprolactone and phthalocyanine derivative for biomedical applications†

Asmaa M. Abd El-Aziz, [a] Eman Serag [bc] and Mohamed E. El-Khouly *[c]

Photodynamic therapy (PDT) is gaining recognition as a promising alternative method for the treatment of diverse biomedical applications. Toward this goal, we report herein the fabrication of an electrospun membrane utilizing polycaprolactone (PCL), and a phthalocyanine derivative, namely 1,4,8,11,15,22,25-octabutyloxy-29*H*,31-phthalocyanine (OBuPc). The designed OBuPc–PCL membrane aims to function as a dressing with the potential to facilitate the management of wound healing. The absorption and fluorescence studies of OBuPc have been examined by the steady-state and time-resolved absorption and fluorescence techniques. From direct detection of the weak emission of the singlet oxygen in the NIR region (at 1270 nm), the quantum yield of singlet oxygen was determined to be 0.05. The physiochemical properties of the nanofibers and membranes that were prepared were determined. The photo-activity of all the modified PCL nanofibers against Gram-positive *S. aureus* and Gram-negative *E. coli* was observed. The PCL/4.8 OBuPc nanofiber exhibited the highest effectiveness, primarily attributed to the enhanced effect of photosensitizer OBuPc as its concentration increased within the fibre. This resulted in *S. aureus* bacterial inhibition% of 62.5% ± 0.38 and 78.5% ± 0.49 after exposure to near infrared emission NIR at 630 nm for 15 minutes and 30 minutes, respectively. The inhibition of *E. coli* bacteria was observed to be 51.51% ± 0.49 and 62.44% ± 0.12% after exposure to near infrared (NIR) emission at a wavelength of 630 nm for durations of 15 minutes and 30 minutes, respectively. Additionally, it was observed that the membranes displayed dark bacterial inhibition. These unique features of the examined nanofibers render them a potential photodynamic antibacterial nanofiber membrane for efficient wound healing treatment and practical antibacterial uses.

Received 23rd May 2024
Accepted 11th July 2024

DOI: 10.1039/d4ra03803g

rsc.li/rsc-advances

1 Introduction

Photodynamic therapy is a highly accurate and minimally invasive procedure employed in the clinical treatment of various malignant and nonmalignant diseases.[1] This approach demonstrated various benefits, including minimal toxicity, precise control, and consistent treatment outcomes.[2] This therapy entails the introduction of photoactive molecules, known as photosensitizers (PSs), along with the application of light and the presence of molecular oxygen in tissues. Individually, these three compounds are not harmful.[3,4] However, when they are combined, they create reactive oxygen species (ROS) such as singlet oxygen ($^1O_2$*), hydrogen peroxide (H_2O_2), superoxide ions ($O_2^{\bullet -}$), or hydroxyl radicals ($OH^{\bullet}$). These ROS cause oxidative damage, leading to the death of target cells.[5]

Several research studies have focused on the use of photodynamic therapy (PDT) to avoid and/or treat infections caused by wounds.[4] PDT has shown significant potential in speeding up the wound healing process. Due to the proliferation of drug-resistant microorganisms, this therapy emerges as a highly promising and effective alternative to antibiotics.[6] However, PS has several drawbacks that must be considered, such as insufficient chemical stability, inability to dissolve in water, and a tendency to self-agglomerate in physiological conditions. The limitations greatly hinder the ability to produce reactive oxygen species (ROS), thereby impeding the use of PS in wound care.[7] Currently, the strategy of integrating PS with carriers has been successfully employed as a highly efficient solution to address a problem. Electrospun nanofibrous membranes (NFMs)

[a]*Fabrication Technology Research Department, Advanced Technology and New Materials Research Institute (ATNMRI), City of Scientific Research and Technological Applications (SRTA-City), Alexandria, Egypt*

[b]*Marine Pollution Department, Environmental Division, National Institute of Oceanography and Fisheries, Kayet Bey, Elanfoushy, Alexandria, Egypt*

[c]*Nanoscience Program, Institute of Basic and Applied Science, Egypt-Japan University of Science and Technology (E-JUST), Alexandria, Egypt. E-mail: mohamed.elkhouly@ejust.edu.eg*

† Electronic supplementary information (ESI) available. See DOI: https://doi.org/10.1039/d4ra03803g

possess significant advantages such as the capacity to regulate pore size, a substantial specific surface area, and the capability to facilitate the passage of oxygen. These characteristics promote the attachment of cells and accelerate their proliferation.[8]

The use of biodegradable nanofibers containing PSs in the development of DDS holds potential as a therapeutic strategy for achieving targeted and controlled drug delivery over a specific period of time.[9] This method ensures that the exact amount of medication is consistently present at the intended location for the necessary duration. Moreover, the structure of the nanofiber mats can mimic the extracellular matrix (ECM) and create a conducive environment for cell growth. Consequently, this promotes the growth of new skin cells and speeds up the process of healing.[10]

Several research studies have focused on the use of PDT to prevent and/or treat infections associated with wounds, which has been found to significantly expedite the wound healing process. Gutberlet, *et al.* developed a platform using poly(D,L-lactide) nanofibers incorporating curcumin and indocyanine green. This platform is designed specifically for antimicrobial therapy. The antimicrobial activity was assessed against *Staphylococcus saprophyticus* subsp. *bovis* and *Escherichia coli* DH5 alpha. The nanofibers, which contained both photosensitizers and were exposed to both wavelengths, resulted in a ($\sim$4.4 $\log_{10}$, 99.996%) reduction in bacterial viability, equivalent to a 99.996% decrease. In comparison, nanofibers loaded with only one photosensitizer or exposed to only one wavelength showed a less significant reduction of less than ($<$1.7 $\log_{10}$, 97.828%). In addition, our formulation successfully eradicated persistent adhered bacteria by more than ($>$4.3 $\log_{10}$, 99.995%).[11]

Previous studies have demonstrated that phthalocyanines, chlorins and their derivatives (PCs) can be utilized to deactivate bacteria in photodynamic therapy (PDT).[12] Several metal-free and metallophthalocyanines were examined for their antibacterial activity, and it was observed that these phthalocyanines possess photoinactivation properties.[12] Kocaağa *et al.* conducted a synthesis of Schiff base substituted phthalocyanine complexes (Zn1c, Zn2c) and their quaternized derivatives (Q-Zn1c, Q-Zn2c), which exhibit considerable potential as photosensitizers for photodynamic therapy (PDT) targeting PC3 cell lines.[13]

The objective of this work was to develop a novel photodynamic antibacterial nanofiber membrane for the treatment of infected wounds. To achieve this objective, this study sought to assess the effects of varying concentrations of octabutyloxy phthalocyanine (OBuPc) as a photosensitizer for photodynamic therapy (PDT) loaded on polycaprolactone nanofiber membranes. The utilization of OBuPc in this study can be rationalized by its strong light absorption in the UV-visible-near infrared regions, as well as other unique physical and chemical properties. The antimicrobial activity of nanofiber membranes was examined against Gram-positive *S. aureus* and Gram-negative *E. coli* bacteria as model organisms. The specific surface area and porosity of the synthesized nanofibers were exceptionally high. They facilitate the healing process by replicating the intricate three-dimensional architecture of the natural cytoplasmic matrix. A novel method for healing infected wounds has emerged by combining the advantages of electrospinning nanofibers with the singlet-oxygen photosensitizer.

2 Material and methods

2.1. Materials

Polycaprolactone with a molecular weight of 80 000 g mol^{-1} and 1,4,8,11,15,18,22,25-octabutyloxy-29*H*,31*H*-phthalocyanine (OBuPc) was obtained from Aldrich Chemicals. Dimethyl sulfoxide (DMSO), tetrahydrofuran (THF), and dimethylformamide (DMF) were purchased from Merck. Chloroform and methanol were also obtained from Merck. The strains *E. coli* (ATCC 25922) and *S. aureus* (ATCC 25923), nutrient broth, and agar bacteriological BBL Muller Hinton were purchased from Davies Diagnostics.

2.2. Preparation of polycaprolactone nanofiber composites

A polymeric solution was prepared by dissolving polycaprolactone (PCL) with a molecular weight of 80 000 g mol^{-1} in a mixture of chloroform and methanol in a ratio of 3 : 1. The resulting solution had a final concentration of 15% by weight. A 20 mL syringe with a blunt-end needle was used to transfer the polymer solution into the electrospinning setup. A high voltage was applied between the tip of the needle and the grounded target (collector) to electrostatically draw the polymer solution from the tip of the needle. The optimization of the solution flow rate for nanostructured fibres was conducted at a rate of 1.0 mL h^{-1}, with an applied voltage of 20 kV and a needle tip and collector distance (air gap) of 15 cm. The outcome derived from this procedure is referred to as control or unmodified (PCL-NF). The PCL solution was supplemented with phthalocyanine nanoparticles at varying concentrations (0.9×10^{-4}, 1.8×10^{-4}, 4.6×10^{-4}) g mL^{-1}. The same parameters have been utilized to achieve the electrospinning process.

2.3. Characterization of prepared nanofiber composites

The optical absorption and fluorescence spectra of OBuPc were performed using UV-Vis-NIR spectrophotometer (Shimadzu model UV-2600) and spectrofluorometer (Shimadzu model RF-6000), respectively. The weak emission band of singlet oxygen *via* the triplet OBuPc was recorded using TCSPC technique (FluoTime 300, PicoQuant, Germany) equipped with NIR-PMT detector with spectra range of 950–1400 nm. LDH-P-C-640B laser head for picosecond pulses was used as an excitation source. The morphology of the nanofiber samples was analyzed using a scanning electron microscope (SEM JEOL JSM 6360LA, Japan) and transmission electron microscopy (JEOL 2100 PLUS, Japan). The Bruker Alpha IR (100 FT-IR) spectrophotometer was used to record the infrared (IR) spectra. The hydrophilicity of the nanofibers was assessed through static contact angle measurement, specifically by examining the right/left drop phase (water) in relation to the external phase (air) and the solid phase (polyethylene).

X-ray diffraction (XRD) analysis was performed on OBUPC and nanofiber membranes using the X-ray 7000 Shimadzu-Japan. The degree of crystallinity of the prepared materials was determined by measuring the Bragg angle (2θ) within the range of 10 to 80°. The X-ray source consists of a copper target that operates at a scan speed of 4° per minute. A voltage of 30 kV a current of 30 mA powers it. The tensile properties of the material were examined using a universal testing machine (AG-I model, Shimadzu, Kyoto, Japan). The nanofiber membranes were divided into rectangular pieces measuring 5 cm in length, 5 cm in width, and 0.8 mL in thickness. Subsequently, these rectangular objects underwent evaluations of their stress–strain curves under tensile conditions.

Thermogravimetric analysis (SDT module-TGA) was used to assess the thermal stability of the polymer that was prepared. Thermogravimetric analysis (TGA) is a testing method used to measure the weight loss of samples (5 mg) in response to changes in temperature. This analysis is conducted using a TGA-50 instrument manufactured by Shimadzu in Japan. The experiment was conducted within a temperature range of 20 to 200 °C, with a heating rate of 10 °C per minute, and under a nitrogen flow rate of 20 mL per minute. Geometry optimizations were carried out using the Becke3LYP functional and the 6-311G basis set, with the restricted Hartree–Fock (RHF) formalism and as implemented in the Gaussian 16 (Revision A.03) software package. Graphical outputs of the computational results were generated with the Gauss View software program (ver. 16) developed by Semichem, Inc.

2.4. Physiochemical characterization

2.4.1 Porosity test. The porosity of nanofiber composites was determined using the Image J software for scanning electron microscopy (SEM) images taken at 100 randomly selected locations. The measurement of membrane thickness was conducted using a micrometre. The membrane's apparent density and porosity were determined using eqn (1) and (2), respectively.

$$\text{Apparent density}\left(\text{g cm}^{-3}\right) = \frac{\text{mass of membrane(g)}}{\text{membrane thickness(cm)} \times \text{membrane area(cm}^2\text{)}} \quad (1)$$

$$\text{Porosity}(\%) = \left(1 - \frac{\text{apparent density(g cm}^{-3}\text{)}}{\text{bulk density(g cm}^{-3}\text{)}}\right) \times 100 \quad (2)$$

2.4.2 Test for swelling. The nanofiber mats were immersed in water for a predetermined duration at ambient temperature. Subsequently, the samples are extracted and subjected to blotting using filter paper prior to weighing. The swelling test was replicated three times for each sample. The swelling percentage of each nanofiber mat is calculated using eqn (3).[14]

$$\text{Swelling}\% = \left(\frac{W_s - W_d}{W_s}\right) \times 100 \quad (3)$$

The weight of the nanofibers after soaking at a specific time interval and subsequent drying is denoted as W_d, whereas the weight of the swollen nanofibers at a specific time is represented as W_s.

2.4.3 The roughness test. The nanofiber mats' surface roughness was assessed by employing a surface roughness tester (SJ-201P, Japan). A set of nanofiber mats measuring 25 mm × 25 mm were fixed onto a glass slide using double-sided tape. The measurements were conducted in three replicates, with each replicate consisting of three samples ($n = 3$).

2.4.4 Hemocompatibility test. The biocompatibility of the prepared NFs membranes was evaluated through a hemolysis test, which quantified the release of haemoglobin caused by the interaction between red blood cells (RBCs) and the tested NFs membranes. The hemolysis test is performed following the guidelines established by the American Society for Testing and Materials (ASTM) in document F756-00, published in 2000.[15] In brief, a recently acquired blood sample from a rabbit was combined with an anticoagulant called EDTA to produce an ACD blood sample. Before coming into contact with rabbit blood, each membrane (1 cm^2) was submerged in a test tube filled with 7 mL of phosphate buffer solution (PBS) with a pH of 7.0. The immersion took place at a temperature of 37 °C for a period of 72 hours. The nanofiber membranes were incubated with 1 mL blood samples at a temperature of 37 °C for 3 hours. The blood samples were subjected to centrifugation at a speed of 2000 RPM for 15 minutes. The supernatant was collected for analysis using UV spectroscopy. The measurement of absorbance was performed at a wavelength of 540 nm in order to assess the concentration of released hemoglobin. The negative and positive controls were generated by combining equal amounts of ACD blood with 7 mL of PBS and water, respectively. The experiments on blood hemolysis were done three times under the same conditions, and eqn (4) was used to figure out the percentage of hemolysis.

$$\text{Hemolysis}\% = \left(\frac{OD_s - OD_n}{OD_p - OD_n}\right) \times 100 \quad (4)$$

OD_s represent the optical density of the sample being tested, OD_n represents the optical density of the negative control, and OD_p represents the optical density of the positive control.

2.4.5 Thrombogenicity test. The development of thrombus on the surface of the developed membranes was assessed using a gravimetric method.[16] The matrices were initially submerged in PBS and subjected to incubation at 37 °C for 48 hours. Subsequently, the PBS was extracted, and the ACD rabbit blood was applied onto the surfaces of the objects under investigation. An equivalent quantity of blood was added to an empty Petri dish as a positive control. A volume of 20 μl of a calcium chloride solution with a concentration of 10 M was applied onto the membrane to initiate the blood clotting reaction. The reaction ended after 45 minutes by introducing 5 mL of H_2O. The clots were subsequently rectified using a 5 mL solution of formaldehyde (36%), followed by drying with tissue paper prior to being measured in terms of weight. Each test was supported by three replicates.

2.4.6 Degradation test. The samples' *in vitro* degradation was studied by immersing them in phosphate buffer saline (PBS) (pH = 7.4) at 37 °C. Dry samples, pre-weighed (W_i), were placed in sterile glass test tubes and immersed in 5 mL of PBS. The samples were then incubated for varying durations of time (3, 14, 15 days). Following a particular period of time, the samples were extracted from the PBS solution, rinsed with deionized water, air-dried at room temperature until the mass stabilized, and quantified (W_t). Ultimately, the dry weight of the samples was reevaluated, and the degree of biodegradation was determined using eqn (5).

$$\left(\frac{W_i - W_t}{W_i}\right) \times 100 \quad (5)$$

2.4.7 Photodynamic antibacterial assay. The photodynamic antibacterial ability of PCL and PCL/OBuPc Nanofiber was evaluated using representative strains of Gram-negative *E. coli* (ATCC 25922), and Gram-positive *S. aureus* (ATCC 29213). In summary, the bacterial strains were cultured overnight in Luria–Bertani (LB) medium with agitation at a temperature of 37 °C. Afterwards, the bacterial solution was diluted to a concentration of 107 CFU mL^{-1} using PBS buffer (0.1 M, pH = 7.0). Subsequently, nanofibers were prepared by weighing three pieces of PCL and PCL/OBuPc (10 mg each) and placing them in a 24-well plate with 100 μL of bacterial solution (107 CFU mL^{-1}) which were pre-cultured in the absence of light for 30 minutes and exposed to visible light at a wavelength of 630 nm (100 mW cm^{-2}) for 15 min and 30 min. The control sample was placed in a dark environment for a duration of 60 minutes. Following that, a volume of 0.9 mL of PBS was introduced to each sample, and the bacteria that were attached to the membranes were eliminated through sonication for a duration of 15 minutes. Subsequently, the bacteria supernatant was diluted with PBS using a 10-fold gradient, and 100 μL of each dilution gradient was inoculated onto LB agar plates. The agar plate that had undergone treatment was placed in an incubator with a constant temperature and humidity of 37 °C for a duration of 18–24 hours. The colonies on the agar plate were quantified to assess its photodynamic antibacterial efficacy. This procedure was repeated three times for each sample.

2.4.8 Biocompatibility studies. For this experiment, we utilized Human Peripheral Blood Mononuclear Cells (PBMCs) that were purified following a specified reference protocol.[17] PCL and PCL/OBuPc nanofibers with 10 mm in diameter (circle shape) were excised and positioned within a 96-well plate (TC Plate, Standard F, Sarstedt). The cells were placed in each well at a density of 300 000 cells per well. The well plate was placed in an incubator and kept at a temperature of 37 °C with a 5% concentration of CO_2 for the purpose of allowing the cells to attach to the fibres. After a period of 48 hours, the medium was taken out and 250 μL of MTT reagent with a concentration of 0.2 mg mL^{-1} was introduced into each well. The specimens were placed in a controlled environment with a temperature of 37 °C and a carbon dioxide concentration of 5% for a duration of 2 hours. Subsequently, the MTT reagent was cautiously eliminated, and the formazan crystals were dissolved in 0.5 mL of DMSO by placing the well plate in an incubator shaker (IKA KS 4000 ic control, IKAWerke GmbH & Co. KG, Staufen, Germany) at a speed of 150 revolutions per minute and a temperature of 37 degrees Celsius for a duration of 20 minutes. A volume of 200 μL of this solution was transferred into a 96-well plate (NUNC, Thermo Fischer Scientific GmbH, Germany), and the absorbance was determined at a wavelength of 490 nm using a plate reader (Microplate reader Biored, Germany). The viability of cells incubated with medium was 100%, while a positive control was established using 0.1% Triton X.

$$\text{Cell viability}\% = OD_{treated}/OD_{control} \quad (6)$$

A OD treated represents the test sample's experimental absorbance (nanofiber membrane + cell), and a OD control positive represents the positive control absorbance (media + cells).

2.4.9 Statistical analysis. Data is presented as mean and standard deviation, conducted using Origin pro software. The statistical significance between groups was determined using one-way analysis of variance (ANOVA). A significance level at of $p < 0.05$ was deemed to be statistically significant.

3 Results and discussion

3.1. Photophysical studies of OBuPc

The molecular geometry of OBuPc, was performed by using *ab initio* B3LYP/6-311G methods. For this, in a first step, the starting moieties, OBuPc was fully optimized to a stationary point on the Born–Oppenheimer potential energy surface and allowed to interact. In the optimized structure, the N–N distance between the four central nitrogen atoms in the cavity was found to be 4.07 Å, while the edge-to-edge distance was found to be 12.97 Å. To gain insights into the molecular geometry of OBuPc, computational studies were performed by using *ab initio* B3LYP/6-311G methods (Fig. S1†). For this, in a first step, the starting moieties, OBuPc was fully optimized to a stationary point on the Born–Oppenheimer potential energy surface and allowed to interact. In the optimized structure, the N–N distance between the four central nitrogen atoms in the cavity was found to be 4.07 Å, while the edge-to-edge distance was found to be 12.97 Å. The highest occupied molecular orbitals (HOMOs) were found to be 4.56 eV, while the energy of the lowest unoccupied molecular orbital (LUMO) was found to be 2.69 eV. Based on these values, the HOMO–LUMO gaps was determined to be 1.86 eV.

The optical absorption and emission studies of OBuPc have been recorded in DMSO to check its ability to absorb and emit the light in the visible-NIR regions. As shown in Fig. 1a, the absorption spectrum of OBuPc exhibited an intense Q-band in the red end of the visible spectrum of light between 600–700 nm with a maximum at 762 nm, and B-bands at 435 and 329 nm.[18] The intense Q-band arises from a doubly degenerate π–π*-transition between the $A_{1g}(a_{1u}^2)$ ground state to the first excited single state, which has $E_u(a_{1u}^1 e_g^1)$ symmetry, while the second allowed π–π* transition (B-band) is due to a transition between either an a_{2u} or a b_{2u} orbital to the e_g orbital (LUMO). As

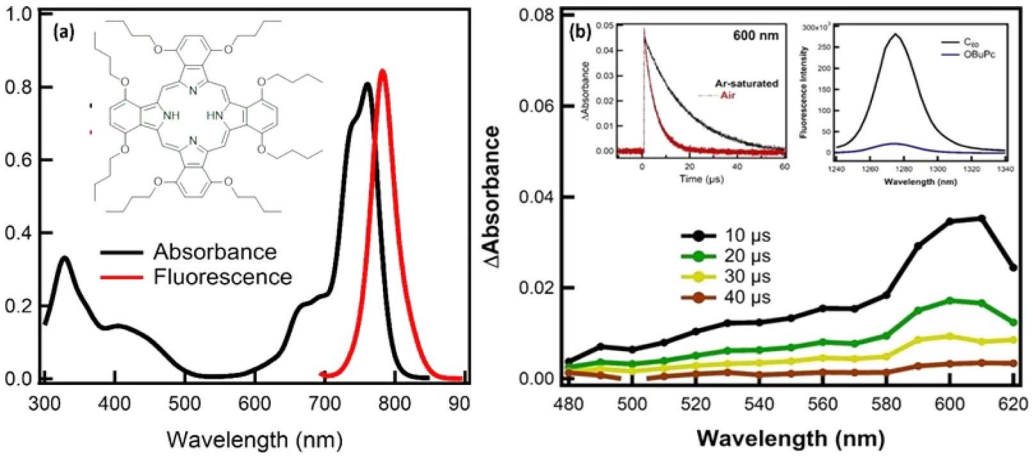

Fig. 1 (a) Absorption and fluorescence spectra of OBuPc in DMSO; inset: molecular structure of OBuPc. (b) Nanosecond transient absorption spectra at the indicated time intervals of OBuPc in argon saturated DMSO. Insets: (Left) Decay profiles of the triplet OBuPc in argon saturated and air saturated DMSO. (Right) Emission spectra of the generated singlet oxygen for the examined OBuPc and the standard C_{60} in air saturated DMSO solutions.

reported in the case of metal-free phthalocyanine derivatives, all states are non-degenerated due to the reduced D_{2h} molecular symmetry.[18] The Q-band transition is polarized in either the *x* or *y* direction, and is therefore split into two bands. Upon photo-excitation of OBuPc with 640 nm excitation light, the fluorescence spectrum of OBuPc displayed a prominent fluorescence peak at 783 nm. From the fluorescence maximum wavelength, the energy of the singlet-excited state of OBuPc was determined to be 1.58 eV.[18]

To get information about the triplet excited state of OBuPc, complementary nanosecond laser photolysis measurements have been performed in argon saturated DMSO using 615 nm excitation light (Fig. 1b). The transient absorption spectra of OBuPc exhibited absorption in the range of 400–650 nm with maximum band at 600 nm that attributed to the triplet–triplet transition of OBuPc. From the decay profile at 600 nm, the rate constant of T–T transition was found to be $5.66 \times 10^4\ s^{-1}$. Based on the rate constant, the lifetime of the triplet OBuPc was calculated to be 17.7 μs. It should be noted the decay profile of the triplet OBuPc was accelerated in the presence of air-saturated DMSO, where the rate constant and lifetime of the triplet state were determined to be $2.07 \times 10^5\ s^{-1}$ and 4.80 μs, respectively. This significant quenching of the triplet excited state of OBuPc is attributed to the energy transfer from the triplet OBuPc to O_2 generating the singlet oxygen ($^1O_2$), as chief cytotoxic species, which subsequently damages cancer cells during the PDT activation.[19–21] The quantity of the singlet oxygen quantum yield is a sign of the capability of the compounds to act as photosensitizers in photodynamic therapy of cancer applications.[19–21] As shown in the inset Fig. 1b, the quantum yield of singlet oxygen (Φ_Δ) of the examined OBuPc was determined to be 0.05 by direct observing the characteristic weak emission band of $^1O_2$ in the near-infrared region with a maximum at 1270 nm and comparing it with Φ_Δ of the standard C_{60}.[19]

3.2. Morphological and characterization of PCL nanofiber and PCL/OBuPc nanofiber membranes

Poly(caprolactone) (PCL) and OBuPc were utilized to fabricate a nanofiber membrane that mimics the characteristics of the extracellular matrix (ECM) and developing a flexible and biologically active substance that can enhance the process of wound healing. Nanofibers of PCL and PCL/OBuPc were fabricated using the electrospinning technique. The successful achievement of producing nanofibers with a consistent structure and the absence of beads was attained by employing our optimized electrospinning parameters. Fig. 2 depicts the scanning electron microscopy (SEM) analysis of the matrices for PCL and PCL/OBuPc. The nanofibers displayed a random orientation and their lengths ranged from several micrometres, the diameters of the samples exhibited variation, with pure PCL NF measuring 343.9 nm, PCL/0.09 OBuPc NF measuring 562 nm, PCL/1.8 OBuPc NF measuring 822.17 nm, and PCL/4.6 OBuPc measuring 864.82 nm. Furthermore, the pure PCL nanofibers displayed a smooth surface texture. The identification of OBuPc particles was observed upon examination of images (c), (e) as well as (g) in Fig. 2.

Fig. 3 displays the utilization of transmission electron microscopy (TEM) and energy-dispersive X-ray spectroscopy (EDS) mapping techniques to validate the incorporation of OBUPC into PCL nanofibers. The findings of this study indicate that the distribution of OBuPc on the nanofibers was uniform.

The infrared spectra of PCL and PCL/OBuPc matrices are illustrated in Fig. 4. Based on the data presented in Fig. 4a, it can be observed that the absorption bands observed at 2951 and 2860 cm^{-1} in PCL are indicative of the stretching vibrations associated with asymmetric CH_2 and symmetric CH_2, respectively.[22,23] The adsorption band observed at 1722 cm^{-1} corresponds to the carbonyl group (C=O), whereas the C–O and C–C stretching bands are observed at 1296 cm^{-1}.[20] Additionally, the absorption band at 1239 cm^{-1} indicates the asymmetric stretching of the C–O–C bond.[24] Otherwise, PCL/OBuPc

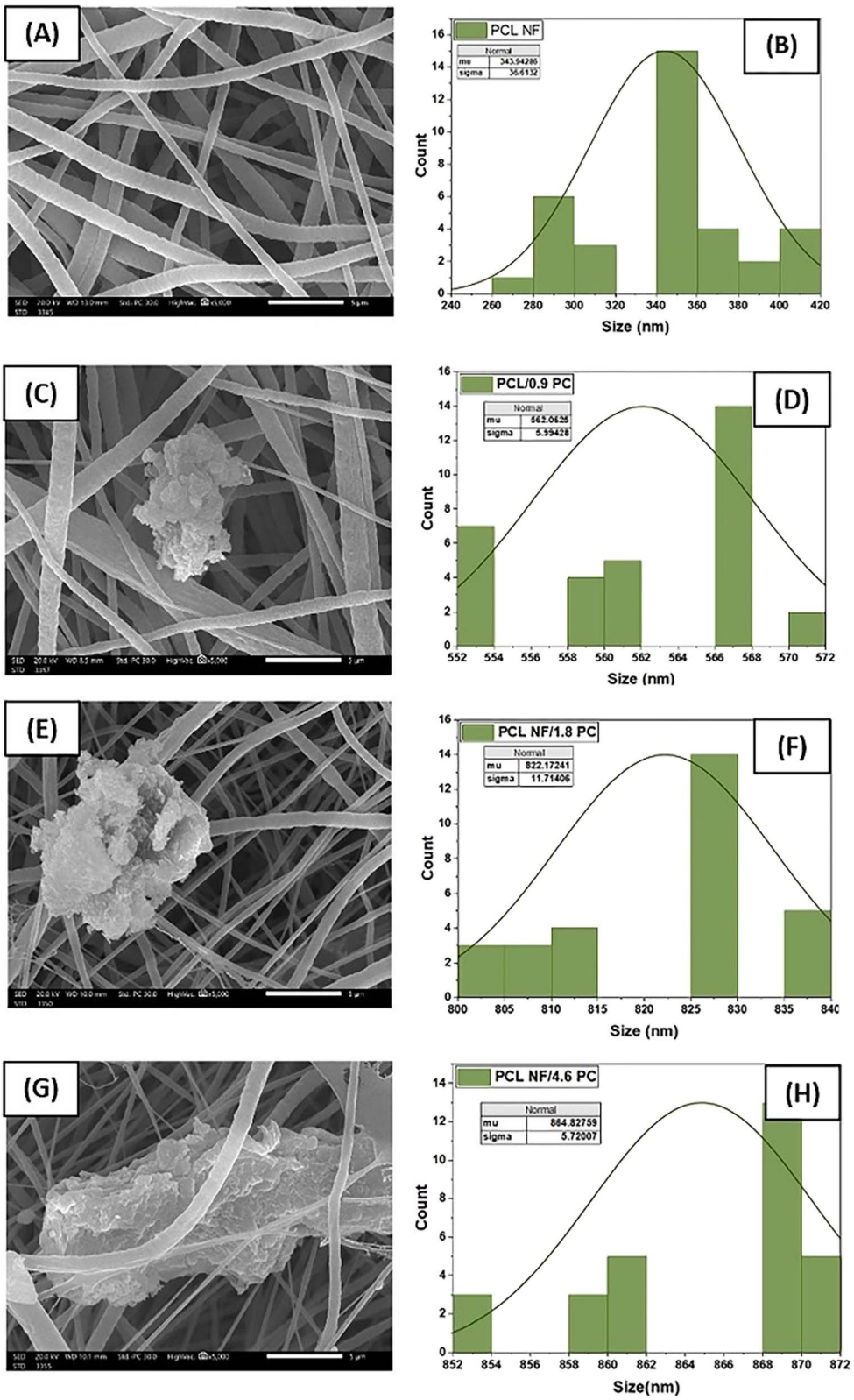

Fig. 2 SEM of the synthesized nanofibers (A), (C), (E) and (G) for PCL, PCL/0.9, PCL/1.8, and PCL/4.6 OBuPc, respectively. (B), (D), (F) , and (H) present the diameter histogram of each membrane, respectively.

nanofibers spectra exhibited different absorption bands, which confirm the incooperation of OBuPc into the fiber. The OBuPc exhibits a range of stretching C–H bands, specifically observed at wavenumbers of 732, 1051, 1011, 1136, 1162, and 1255 cm^{-1}.[21] The observed peaks at dimensions of 721 and 886 cm^{-1} are indicative of out-of-plane C–H bend modes.[25] The

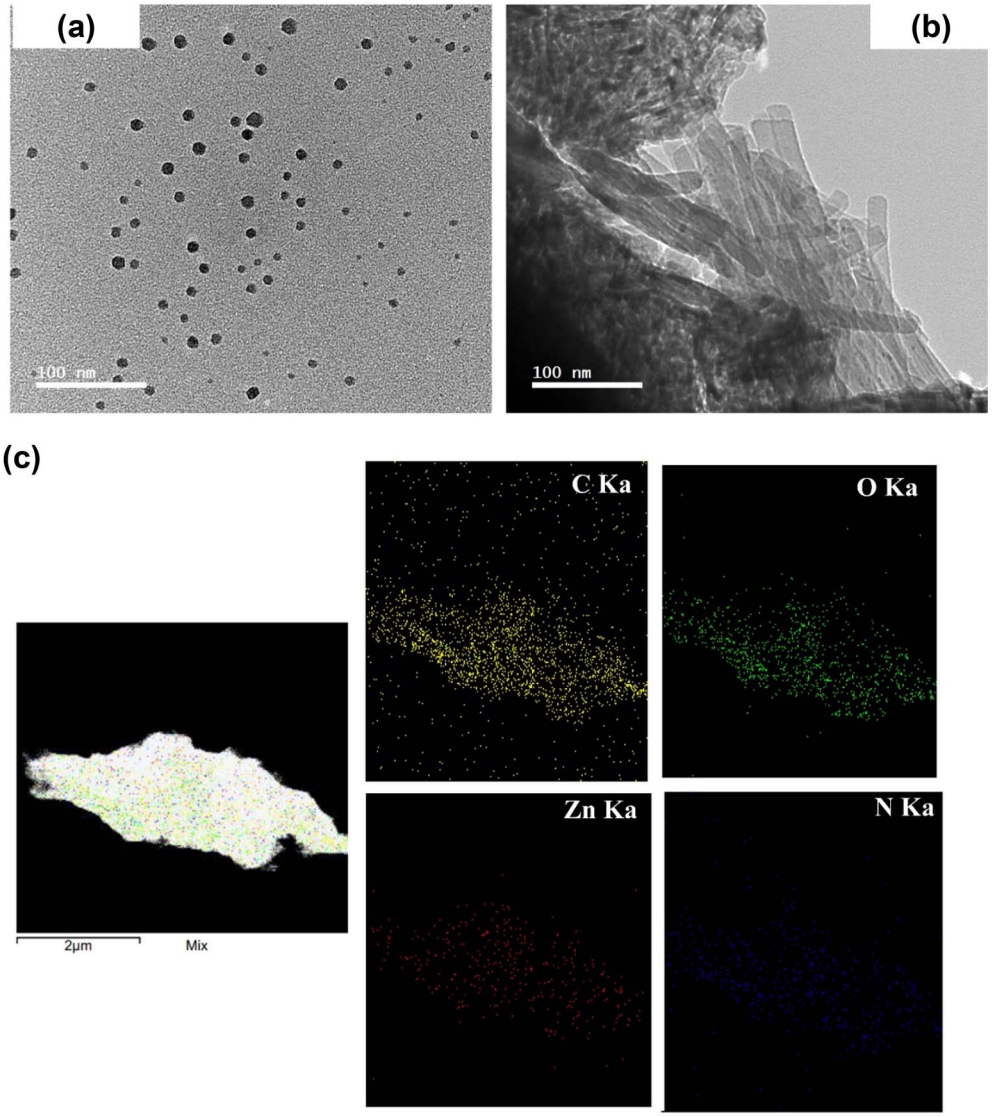

Fig. 3 (a) Transmission electron microscope images of PCL/4.8 OBuPc (a), with a 50 nm zoom on the same nanofiber membrane, and (b) of OBuPc particles. (c) EDS map for PCL/4.8 OBuPc.

bands observed at 1329 and 1408 cm^{-1} correspond to the in-plane stretching of pyrrole and isoindole, respectively.[26] The peaks observed at 1512, and 1706 cm^{-1} are associated with the C–C benzene stretch while C–H of aromatic at 3090 cm^{-1}.[27] The observed peak at 1722 cm^{-1} correspond to the C–H stretching vibration, while C–H stretching vibration was recorded at 3090 cm^{-1}.[28] The presence of observed bands in the PCL/OBuPc nanofiber networks provides confirmation of the successful incorporation of OBuPc into the fibre, which is consistent with the results reported in previous studies.[29,30]

Fig. 4b exhibited the X-ray diffraction (XRD) patterns of PCL nanofiber, PCL/4.8 OBuPc nanofiber membranes, in addition to the PCL nanofiber and OBuPc. For PCL nanofibers, Fig. S1† reveals the presence of two prominent diffraction peaks at Bragg angles of 21.4° and 23.8°, these peaks are in a good agreement with the reported diffraction values of the (110) and (200) lattice planes of semi-crystalline PCL, respectively.[31] The OBuPc pattern exhibits distinct peaks at 23° and 26°.[32] However, when compared to pure PCL fibres, the peak intensity of 21.4° showed significantly decrease in the presence of OBuPc. Therefore, we can conclude that the interaction between nanofibers and OBuPc solely influences the degree of crystallinity without changing the type of PCL crystal nanofibers. We observed the primary peak of PCL at 21.4° and 23.8° for all materials, and the crystal structure remained unaltered. This finding is consistent with previous study.[23]

An investigation was conducted to analyze the decomposition characteristics of pure PCL and PCL 4.8 OBuPc nanofibers in the absence of oxygen. By utilizing thermal gravimetric analysis, as depicted in Fig. S3.† The TGA curves clearly demonstrate that the PCL/4.8 OBuPc nanocomposite fibre undergoes degradation and maximum decomposition at higher temperatures compared to the pure PCL nanofibers. The degradation temperature at which the PCL/4.8 OBuPc

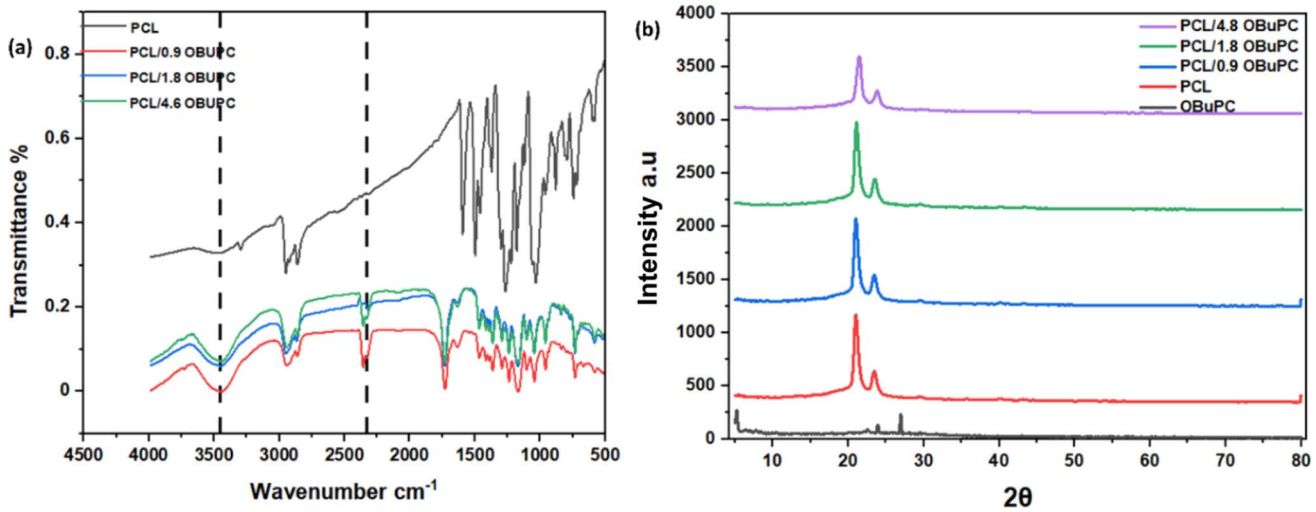

Fig. 4 (a) FTIR, (b) XRD of the synthesized nanofibers membranes.

nanocomposite fibers experience a 5 wt% weight loss increased from 59.39 °C for the pure PCL nanofibers to 61.79 °C for PCL/4.8 OBuPc. In comparison, the maximum temperature (T_{max}) for pure PCL was found to be 190.6 °C, while for PCL/4.8 OBuPc it was found to be 190.9 °C. The thermal decomposition curve of PCL 4.8 OBuPc shifts towards a higher temperature, suggesting that the presence of OBuPc can enhance the thermal stability of PCL nanofibers. The outcome is comparable to that observed in tetraamino phthalocyanine zinc (TAPcZn) micro-crosslinked polyimide films. The incorporation of phthalocyanine rings enhanced the heat resistance of the PI/TAPcZn films.[33]

3.3. Physical and biological properties of nanofiber membranes composites

The contact angle is a crucial factor that influences the surface's wetting capacity and significantly affects its biocompatibility capability. Frequently, the application of hydrophilic coating materials aids in the elimination of biological substances by creating a water layer at the interface.[34] Electrospun fiber contact angle depicted in Fig. 5. The PCL nanofiber demonstrated a contact angle of 86.7 ± 1.61°, as the addition of OBuPc to the PCL nanofibers resulted in a significant increase in the contact angles of the PCL ($p < 0.01$). The contact angle of PCL/0.9 OBuPc, PCL/1.8 OBuPc, PCL/4.8 OBuPc are (106.5 ± 0.56°), (114.5 ± 1.32°) and (116.8 ± 2.58°) nanofibers, respectively. The experimental results demonstrated that the contact angle of PCL fiber exhibits a range of 86 to 120°. This is attributed to electrospun materials have rough, rippled surfaces that trap air between them. This makes the materials water-resistant. As a result, this trapped air keeps liquids, like water, from going through the ripples and stays on top as whole droplets.[35] This result was consistent with the reported work,[30] which found that the hydrophobicity of polyvinyl alcohol and polyethylene nanofiber was increased by incooperative silicon phthalocyanine. When the results of the swelling test were compared to the contact angle results, as shown in Fig. 5a, the swelling ratios decrease with increasing the amounts of OBuPc.

In certain applications, such as wound dressing, there is a need for a layer that possesses both high porosity and effective protection. The permeability of wound dressings to oxygen, regulation of water vapor release, and facilitation of fluid passage are attributed to the elevated porosity within the nanofiber layer, thereby contributing to the process of wound healing.[36] Table 1 presented the porosity and roughness of the nanofiber composites. As listed, the porosity of PCL/4.8 OBuPc and PCL reached a minimum value of 64.84 ± 12.39% and a maximum value of 104.18 ± 7.16%, respectively. The porosities of the PCL/gelatin nanofiber membranes in previous studies have been observed to fall within the range of 60–80%.[32] The regulation of porosity is a crucial factor in the development of a suitable nanofibrous matrix, as it facilitates effective oxygen and nutrient exchange within the wound tissue.[37] The study revealed that the porosity of nanofiber membrane composites with proper percentage and did not have a significant impact on the mechanical properties of the composites.

The roughness parameters of PCL/OBuPc nanofibers are presented in Table 1. The average roughness of nanofibers increases as the ratio of OBuPc increases. The obtained result demonstrates a satisfactory average roughness, as an increase in roughness may impede cell connectivity, while a decrease in roughness may result in reduced cell adhesion to the nanofiber membrane. Otherwise, the previous study employed polyvinyl alcohol and hyaluronic acid as scaffolds, which yielded average roughness values ranging from 3.5 to 5.5 μm across different concentrations of hyaluronic acid.[38]

The physiological stability of nanofibers composites is essential during their application, as the rate of degradation should align with the improvement in functional recovery. The deterioration of the control and nanocomposite nanofibers mats was examined in a PBS solution over a period of 15 days. Table 1, and Fig. S4† demonstrated that the inclusion of OBuPc in the scaffolds resulted in a notable reduction in the rate of degradation. The degradation rates of the scaffolds were found to be dependent on the OBuPc contents. As an illustration, the

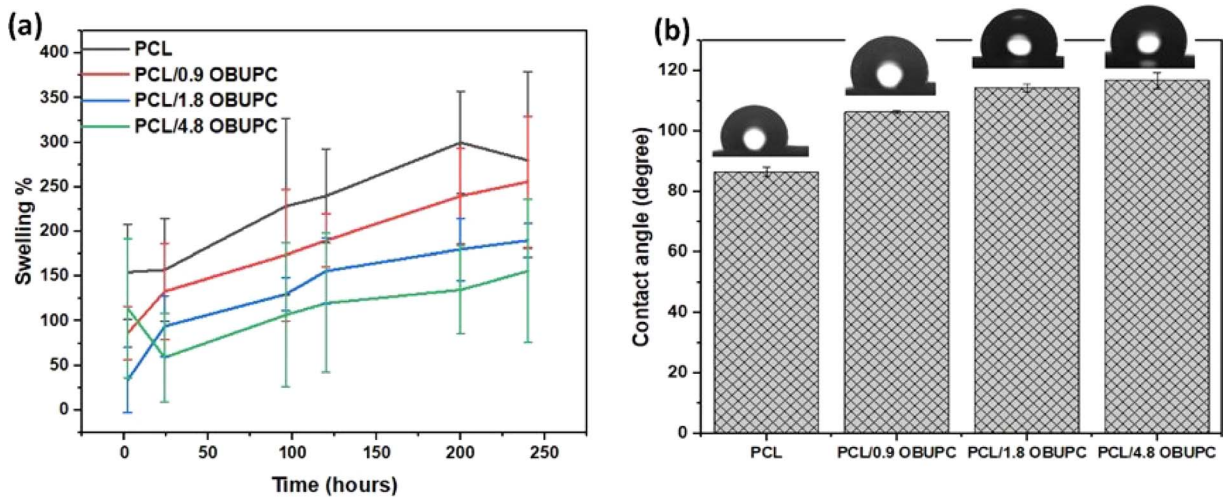

Fig. 5 Swelling test (a) and contact angle (b) of PCL nanofiber membranes composites.

control nanofiber exhibited a degradation rate of 20.59%, 20%, and 23.45% on the third, tenth, and fifteenth days, respectively. While, the 4.6 PCL nanofibers scaffold exhibited a degradation rate of 12.72, 13.34, and 14.82%, respectively. This phenomenon can be attributed to the interactions between the polymer and the OBuPc, which result in the formation of a nanofibers structure that is both more stable and compact.[39] The increased stability due to the compact and intricate network that is created when OBuPc is incorporated into PCL. Moreover, the observed decrease in degradation is in line with previous research that has shown BBG-based scaffolds to exhibit reduced degradation.[40]

In addition, nanofibers' mechanical strength and formability greatly affect cell morphology-related processes including migration, proliferation, and differentiation.[41] Therefore, the tensile strength of the nanofiber composites that were prepared was measured and is illustrated in Fig. 6. The addition of various concentrations of OBuPc resulted in enhanced mechanical properties of the nanofibers. Specifically, the young modulus of pure PCL fibre was measured to be 9.068 ± 0.11, PCL/0.9 OBuPc was found to be 10.7 ± 0.34, PCL/1.8 OBuPc was determined to be 24 ± 0.56, and PCL/4.8 OBuPc was measured to be 28.5 ± 0.43. The obtained results match with the human skin tensile strength which is about 1–40 MPa. Otherwise the behavior of the nanofiber membrane composites in tensile strength exhibit similarities to those obtained through the functionalization of polystyrene superfine fibre with copper phthalocyanine.[42] Otherwise chitosan (Cs)-polycaprolactone (PCL)/polyvinylalcohol (PVA)-melatonin (MEL)/chitosan-polycaprolactone three-layer nanofiber wound dressing was designed and provide tensile strength (14.21 MPa).[43]

3.4. Hemocompatibility studies

Biomaterials coming into contact with blood, whether directly or indirectly, need to have their blood compatibility evaluated. The hemolysis test holds significant importance as an *in vitro* preliminary screening and assessment of blood compatibility. The hemolytic percentages of the nanofiber mats investigated are depicted in Fig. 7a. The results of the study indicated a tiny boost in hemolytic efficiency when comparing the modified and unmodified membranes. Nevertheless, the observed hemolysis rate in all the samples that were prepared remains below 2%, a threshold deemed safe according to the ASTM F 756-00, 2000 standard. The compatibility of PCL/OBuPc nanofiber mats with non-hemolysis materials was observed and these findings align with prior research and are consistent with the results reported in previous studies.[44,45]

An important property of the material for wound healing is its thrombogenicity. In comparison to the PCL/OBuPc nanofiber membranes, the PCL nanofiber showed a decreased tendency for thrombus formation (Fig. 7b). Previous research has shown that photodynamic photosensitizers can improve the procoagulation capabilities of endothelial cells.[46–48] As a result, using PCL/OBuPc nanofibers as a biodressing material to keep

Table 1 The porosity, roughness, and biodegradability of the nanofiber composites

			Degradation, %		
Samples	Porosity, %	Roughness, μm	3 days	10 days	15 days
PCL	104.18 ± 7.16	0.639091 ± 0.423614	20.59 ± 12.61	20.0 ± 8.99	23.45 ± 10.15
PCL/0.9 OBuPc	90.5 ± 15.45	0.931818 ± 0.216278	11.45 ± 7.365	12.33 ± 6.128	15.47 ± 1.68
PCL/1.8 OBuPc	94.18 ± 19.32	1.266667 ± 0.199423	10.34 ± 11.12	10.71 ± 1.46	11.59 ± 2.18
PCL/4.8 OBuPc	64.84 ± 12.39	1.882727 ± 0.562585	12.72 ± 12.72	13.34 ± 3.87	14.82 ± 4.50

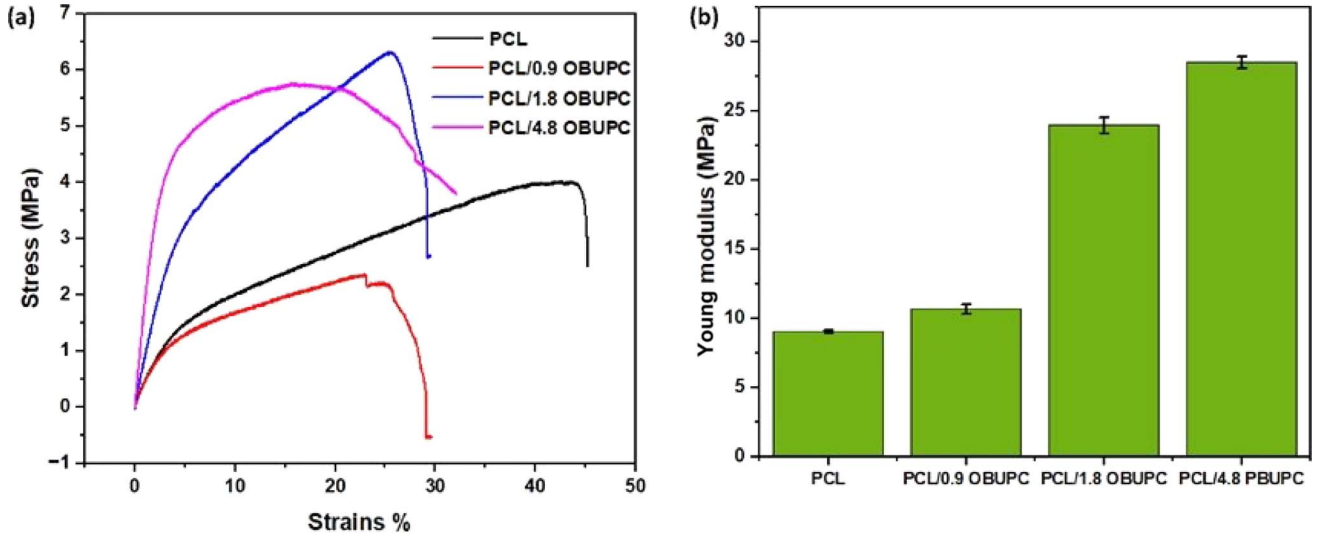

Fig. 6 (a) Stress–strain% curve, (b) Young modulus for nanofiber membranes composites.

wounds moist and maintain mechanical integrity while they heal has shown remarkable effectiveness.

3.5. Photodynamic inactivation of *Staphylococcus aureus*, and *Escherichia coli*

An investigation was conducted to evaluate the photodynamic efficiency of PCL/OBuPc nanofiber against *Staphylococcus aureus* and *Escherichia coli*. The effectiveness of nanofibers in inhibiting the growth of *S. aureus* and *E. coli* was assessed by subjecting them to red light exposure (with a wavelength of 630 nm) for durations of 15 and 30 minutes, as depicted in Fig. 8a–d. The obtained results are expressed in bacteria account $\log_{10}$ CFU mL^{-1} and bacterial survival%.

A comparison was made between the photodynamic efficiency of all nanofiber samples and that of the control in dark conditions. It was observed that there was no significant decrease in the activation of bacterial strains in dark conditions compared to light conditions. However, the efficiency of photodynamic activation was affected by the duration of exposure to light radiation. However, it should be noted that PCL nanofiber membranes containing higher concentrations of OBuPc exhibited greater inhibition of bacterial growth. Specifically, PCL/4.9 OBuPc resulted in a reduction of 1.95424 ± 0.213 log CFU mL^{-1} in Gram-positive *S. aureus*, while PCL/0.9 OBuPc led to a reduction of approximately 5.81291 ± 0.324 log CFU mL^{-1} in Gram-positive *S. aureus* after being exposed to near-infrared (NIR) radiation for a duration of 30 minutes. In contrast, the usage of PCL/4.9 OBuPc resulted in a decrease in the population of Gram-negative *E. coli* by 2.10309 ± 0.495 log CFU mL^{-1}, whereas the use of PCL/0.9 OBuPc led to a reduction in Gram-negative *E. coli* by approximately 4.65321 ± 0.654 log

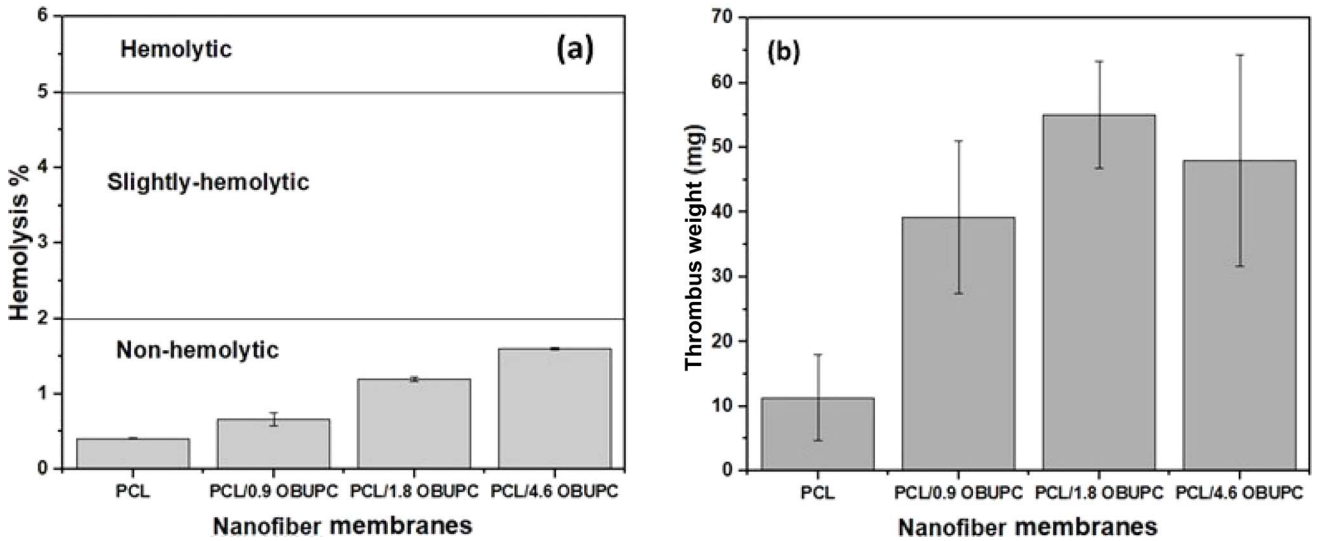

Fig. 7 (a) The hemolysis analysis, and (b) thrombus analysis for the nanofiber membranes composites.

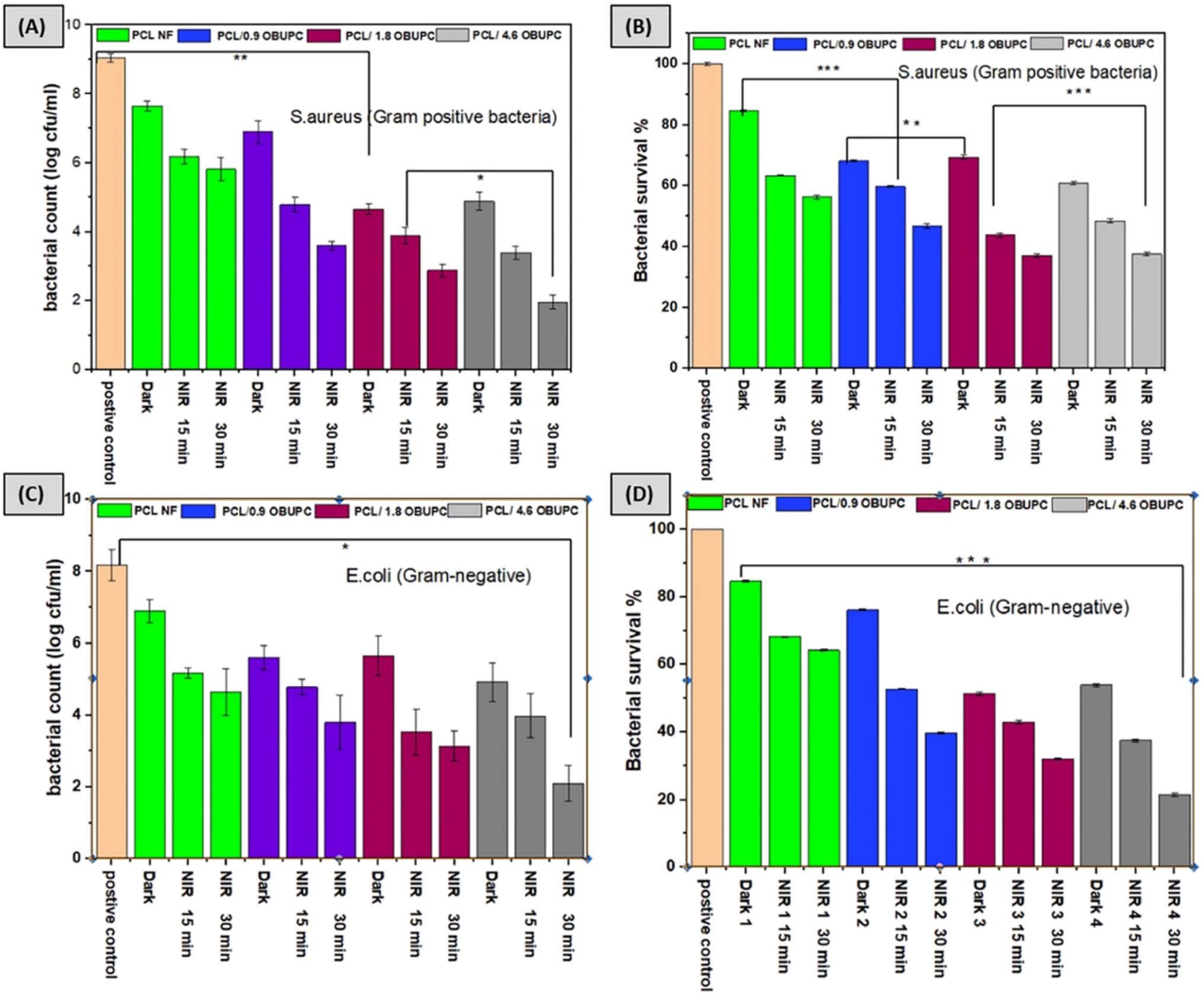

Fig. 8 The effect of nanofibers membranes composites on (A) the account, (B) the survival% of Gram-positive *S. aureus*. The effect of nanofibers membranes on the account (C) and (D) survival% of Gram-negative *E. coli*. Data are presented as means ± SD ($n = 3$, *$p < 0.05$, **$p < 0.01$, and ***$p < 0.001$).

CFU mL^{-1} following a 30 minute exposure to near-infrared NIR radiation. The findings highlight the significance of the production of singlet oxygen ($^1O_2$) by the PS.

After being exposed to near-infrared (NIR) radiation, OBuPc has the potential to generate singlet oxygen, which can lead to damage to the outer membrane of bacteria. This damage can impact the permeabilization of the bacterial cytomembrane and ultimately compromise the integrity of the bacteria. The cytomembrane of *Escherichia coli* was disrupted, resulting in significant leakage of cytoplasm. Bacterial death results from the disruption of the bacterial membrane, which also causes the loss of structural integrity and membrane function.[49] On the other hand, the cell wall of Gram-positive bacteria is composed of lipoteichoic and teichoic acids, which are arranged in several layers of peptidoglycan.[50] The permeability of this envelope is enhanced, thereby promoting the photodynamic activity of photodynamics on bacterial cells. Gram-negative bacteria have a cell wall composed of an intricate outer membrane made up of phospholipids, lipopolysaccharides, lipoteichoic acids, and lipoproteins. This envelop forms a selectively impermeable protective barrier against multiple antimicrobial agents.[51] That explains why the nanofibers were slightly more effective in killing *S. aureus* than *E. coli*.

3.6. The compatibility of nanofiber materials

The nanofiber formulations were assessed for cellular biocompatibility using Human Peripheral Blood Mononuclear Cells (PBMCs), as shown in Fig. 9. None of the nanofiber membranes exhibited significant toxicity, with the lowest survival rate of 71.8% observed for the PCL/1.8 OBuPc membrane. This phenomenon may be attributed to the fibrous composition of the structure, which closely resembles that of tissue. As a result, the cells are able to settle into the structure in a three-

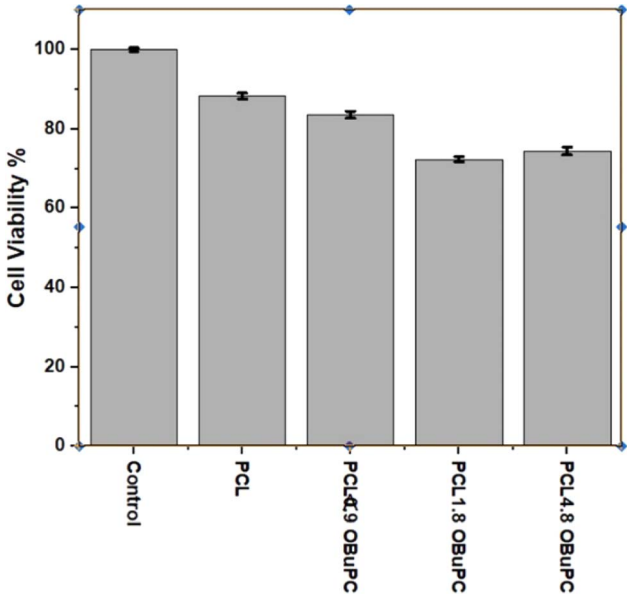

Fig. 9 Cell viability of PBMCs as a contact of the nanofibers mats.

dimensional manner and survive.[11] This phenomenon has frequently been depicted, and it enhances the process of healing wounds on the skin. Overall, the produced formulations did not exhibit any toxicity, indicating their safe usage.

4 Conclusion

Near-infrared absorbing octabutyloxy phthalocyanine has been incorporated polycabrolacton nanofibers (OBuPc/PCL) was successfully prepared by electrospinning a blend solution of PCL/OBuPc particles. The homogeneous distribution of the OBuPc and the porous structure of the nanofibers were demonstrated through various characterizations. The inclusion of OBuPc results in an extended contact angle, reduced hydrophilicity, and improved mechanical characteristics of the nanofibers. Moreover, the incorporation of OBuPc into the fiber leads to an augmentation in the photodynamic antibacterial efficacy against both Gram-positive *S. aureus* and Gram-negative *E. coli* bacteria. These unique features of the synthesized nanofibrous membranes, in addition to their extremely low significant cytotoxicity, render them as potential potentials for the biomedical applications.

Ethical statement

The *in vitro* tests were conducted using human cell lines and was approved by the institutional Research Ethics Committee at E-JUST.

Data availability

The datasets utilized and/or examined in the present study can be obtained from the corresponding author upon a reasonable request. The data supporting this article have been included as part of the ESI.†

Conflicts of interest

The authors declare no conflict of interest.

Acknowledgements

Mohamed E. El-Khouly acknowledges Science, Technology & Innovation Funding Authority (STIFA), Egypt, Project No. 46207 for the financial support.

References

1 X. Liu, Y. Lu, X. Li, L. Luo and J. You, Nanoplatform-enhanced photodynamic therapy for the induction of immunogenic cell death, *J. Controlled Release*, 2024, **365**, 1058–1073.
2 J. Gao, Y. Tian, Y. Li, F. Hu and W. Wu, Design strategies for aggregation-induced emission photosensitizers with enhanced safety in photodynamic therapy, *Coord. Chem. Rev.*, 2024, **507**, 215756.
3 N. Alvarez and A. Sevilla, Current Advances in Photodynamic Therapy (PDT) and the Future Potential of PDT-Combinatorial Cancer Therapies, *Int. J. Mol. Sci.*, 2024, **25**, 1023.
4 K. Zha, W. Zhang, W. Hu, M. Tan, S. Zhang, Y. Yu, S. Gou, P. Bu, B. Zhou, Y. Xiong, B. Mi, G. Liu, Q. Feng and K. Cai, Three-Step Regenerative Strategy: Multifunctional Bilayer Hydrogel for Combined Photothermal/Photodynamic Therapy to Promote Drug-Resistant Bacteria-Infected Wound Healing, *Adv. Funct. Mater.*, 2024, **34**, 2308145.
5 M. Chen, A. Zhou and A. Khachemoune, Photodynamic Therapy in Treating a Subset of Basal Cell Carcinoma: Strengths, Shortcomings, Comparisons with Surgical Modalities, and Potential Role as Adjunctive Therapy, *Am. J. Clin. Dermatol.*, 2024, **25**, 99–118.
6 S. Yaghobee, M. Pourhajibagher, R. Bahrami and M. Isaabadi, Nano-emodin mediated photodynamic therapy for wound healing of donor site after free gingival graft: A parallel clinical trial, *Photodiagn. Photodyn. Ther.*, 2024, **45**, 103958.
7 K. Khorsandi and R. Fekrazad, Skin wound healing in diabetic rat model using low-dose photodynamic therapy, *Biotechnol. Appl. Biochem.*, 2024, **71**, 681–690.
8 J. Li, S. Zhang, C. He and J. Ling, Electrospun fibers based anisotropic silk fibroin film with photodynamic antibacterial therapy for S. aureus infected wound healing, *Int. J. Biol. Macromol.*, 2024, **254**, 127685.
9 M. A. Abdel Khalek, A. M. Abdelhameed and S. Abdel Gaber, The Use of Photoactive Polymeric Nanoparticles and Nanofibers to Generate a Photodynamic-Mediated Antimicrobial Effect, with a Special Emphasis on Chronic Wounds, *Pharmaceutics*, 2024, **16**, 229.
10 E. Bayrak, P. Yiğit, E. Bakay, B. Sirek, N. Topaloğlu, E. Baysoy and G. Kaleli-Can, Accelerating Wound Healing with

Combinatorial Therapy Using Natural Melanin Nanoparticle-Polyvinyl Alcohol Blend and Core-Sheath Hybrid Nanofibers under UV-A Irradiation, *Macromol. Mater. Eng.*, 2024, **309**(5), 2300382.

11 B. Gutberlet, E. Preis, V. Roschenko and U. Bakowsky, Photothermally Controlled Drug Release of Poly(d,l-lactide) Nanofibers Loaded with Indocyanine Green and Curcumin for Efficient Antimicrobial Photodynamic Therapy, *Pharmaceutics*, 2023, **15**, 327.

12 W. Su, X. Luo, P. Li, Y. Zhang, C. Lin, K. Wang and J. Jiang, Phthalocyanine self-assembled nanoparticles for type I photodynamic antibacterial therapy, *Chin. Chem. Lett.*, 2024, 109522.

13 N. Kocaağa, A. Türkkol, M. D. Bilgin and A. Erdoğmuş, The synthesis of novel water-soluble zinc (II) phthalocyanine based photosensitizers and exploring of photodynamic therapy activities on the PC3 cancer cell line, *Photochem. Photobiol. Sci.*, 2023, **22**, 2037–2053.

14 A. M. Abd El-Aziz, A. El-Maghraby, A. Ewald and S. H. Kandil, In-Vitro Cytotoxicity Study: Cell Viability and Cell Morphology of Carbon Nanofibrous Scaffold/Hydroxyapatite Nanocomposites, *Molecules*, 2021, **26**, 1552.

15 E. Serag, A. M. A. El-Aziz, A. El-Maghraby and N. A. Taha, Electrospun non-wovens potential wound dressing material based on polyacrylonitrile/chicken feathers keratin nanofiber, *Sci. Rep.*, 2022, **12**, 15460.

16 T. M. Tamer, M. M. Sabet, A. M. Omer, E. Abbas, A. I. Eid, M. S. Mohy-Eldin and M. A. Hassan, Hemostatic and antibacterial PVA/Kaolin composite sponges loaded with penicillin–streptomycin for wound dressing applications, *Sci. Rep.*, 2021, **11**, 3428.

17 M. C. M. Vissers, S. A. Jester and J. C. Fantone, Rapid purification of human peripheral blood monocytes by centrifugation through Ficoll-Hypaque and Sepracell-MN, *J. Immunol. Methods*, 1988, **110**, 203–207.

18 M. E. El-Khouly, Energy transfer between two light harvesting phthalocyanine derivatives as model for artificial photosynthetic antenna: Laser photolysis studies, *Spectrochim. Acta, Part A*, 2018, **205**, 508–513.

19 K. M. M. Rahman, P. Giram, B. A. Foster and Y. You, Photodynamic Therapy for Bladder Cancers, A Focused Review(†), *Photochem. Photobiol.*, 2023, **99**, 420–436.

20 N. A. Kuznetsova, N. S. Gretsova, V. M. Derkacheva, S. A. Mikhalenko, L. I. Solov'eva, O. A. Yuzhakova, O. L. Kaliya and E. A. Luk'yanets, Generation of Singlet Oxygen with Anionic Aluminum Phthalocyanines in Water, *Russ. J. Gen. Chem.*, 2002, **72**, 300–306.

21 T. Xiong, M. Li, Y. Chen, J. Du, J. Fan and X. Peng, A singlet oxygen self-reporting photosensitizer for cancer phototherapy, *Chem. Sci.*, 2021, **12**, 2515–2520.

22 S. Fahimirad, P. Satei, A. Ganji and H. Abtahi, Polymer Edition, Wound healing performance of PVA/PCL based electrospun nanofiber incorporated green synthetized CuNPs and Quercus infectoria extracts, *J. Biomater. Sci., Polym. Ed.*, 2023, **34**, 277–301.

23 F. Pourhojat, M. Sohrabi, S. Shariati, H. Mahdavi and L. Asadpour, Evaluation of poly ε-caprolactone electrospun nanofibers loaded with Hypericum perforatum extract as a wound dressing, *Res. Chem. Intermed.*, 2017, **43**, 297–320.

24 R. Yaseri, M. Fadaie, E. Mirzaei, H. Samadian and A. Ebrahiminezhad, Surface modification of polycaprolactone nanofibers through hydrolysis and aminolysis: a comparative study on structural characteristics, mechanical properties, and cellular performance, *Sci. Rep.*, 2023, **13**, 9434.

25 Z. U. Islam, M. Tahir, W. A. Syed, F. Aziz, F. Wahab, S. M. Said, M. R. Sarker, S. H. Md Ali and M. F. M. Sabri, Fabrication and photovoltaic properties of organic solar cell based on zinc phthalocyanine, *Energies*, 2020, **13**, 962.

26 H. A. Mohammed and M. M. Kareem, Synthesis and Characterization of New Zinc-phthalocyanine with Four Dodecenyl-benzoic Pendant Groups, *J. Univ. Babylon Pure Appl. Sci.*, 2017, **25**, 486–496.

27 T. Guo, T. Zou, P. Shi, Y. Song, M. Wu, F. Xiao, J. Zhang, W. Wu and H. Wang, A new polymorph of zinc-phthalocyanine and its optical properties, *J. Cryst. Growth*, 2020, **546**, 125760.

28 N. J. D. Fatima, Zinc phthalocyanine compound-based photo-electric organic shock-proof disposable flexible sensors, *Dyes Pigm.*, 2024, **222**, 111772.

29 W. Tong, Y. Xiong, S. Duan, X. Ding and F.-J. Xu, Phthalocyanine functionalized poly(glycidyl methacrylate) nano-assemblies for photodynamic inactivation of bacteria, *Biomater. Sci.*, 2019, **7**, 1905–1918.

30 A. N. Severyukhina, N. V. Petrova, A. M. Yashchenok, D. N. Bratashov, K. Smuda, I. A. Mamonova, N. A. Yurasov, D. M. Puchinyan, R. Georgieva, H. Bäumler, A. Lapanje and D. A. Gorin, Light-induced antibacterial activity of electrospun chitosan-based material containing photosensitizer, *Mater. Sci. Eng., C*, 2017, **70**, 311–316.

31 W. J. Al-Kaabi, S. Albukhaty, A. J. Al-Fartosy, H. K. Al-Karagoly, S. Al-Musawi, G. M. Sulaiman, Y. H. Dewir, M. S. Alwahibi and D. A. Soliman, Development of Inula graveolens (L.) plant extract electrospun/polycaprolactone nanofibers: a novel material for biomedical application, *Appl. Sci.*, 2021, **11**, 828.

32 T. Guo, T. Zou, P. Shi, Y. Song, M. Wu, F. Xiao, J. Zhang, W. Wu and H. Wang, A new polymorph of zinc-phthalocyanine and its optical properties, *J. Cryst. Growth*, 2020, **546**, 125760.

33 Y. Zhang, J. He and R. Yang, Ultra-low dielectric constant and high thermal stability of low-crosslinked polyimide with zinc tetraamino phthalocyanine, *J. Mater. Sci.*, 2022, **57**, 16064–16079.

34 R. R. Choudhury, J. M. Gohil, S. Mohanty and S. K. Nayak, Antifouling, fouling release and antimicrobial materials for surface modification of reverse osmosis and nanofiltration membranes, *J. Mater. Chem. A*, 2018, **6**, 313–333.

35 P. K. Szewczyk, D. P. Ura, S. Metwally, J. Knapczyk-Korczak, M. Gajek, M. M. Marzec, A. Bernasik and U. Stachewicz, Roughness and Fiber Fraction Dominated Wetting of Electrospun Fiber-Based Porous Meshes, *Polymers*, 2019, **11**, 34.

36 A. Sedigheh, in *Biocomposites*, ed. M. M. E. Magdy and K. Selcan, IntechOpen, Rijeka, 2022, ch. 4, DOI: 10.5772/intechopen.109104.
37 A. A. Hassan, H. A. Radwan, S. A. Abdelaal, N. S. Al-Radadi, M. K. Ahmed, K. R. Shoueir and M. A. Hady, Polycaprolactone based electrospun matrices loaded with Ag/hydroxyapatite as wound dressings: Morphology, cell adhesion, and antibacterial activity, *Int. J. Pharm.*, 2021, **593**, 120143.
38 S. Jegina, L. Salaka, S. Kukle, D. Livkisa and J. Gravitis, A preliminary study on sodium hyaluronate loaded polyvinyl alcohol nanofiber webs obtained via roller electrospinning, *IOP Conf. Ser.: Mater. Sci. Eng.*, 2019, **500**, 012024.
39 J.-Y. Park, K.-H. Kyung, K. Tsukada, S.-H. Kim and S. Shiratori, Biodegradable polycaprolactone nanofibres with β-chitosan and calcium carbonate produce a hemostatic effect, *Polymer*, 2017, **123**, 194–202.
40 A. M. Abd El-Aziz, A. Abd El-Fattah, A. El-Maghraby, D. A. Ghareeb and S. Kandil, Viscoelasticity, Mechanical Properties, and In Vitro Bioactivity of Gelatin/Borosilicate Bioactive Glass Nanocomposite Hydrogels as Potential Scaffolds for Bone Regeneration, *Polymers*, 2021, **13**, 2014.
41 J. Yao, C. W. Bastiaansen and T. Peijs, High strength and high modulus electrospun nanofibers, *Fibers*, 2014, **2**, 158–187.
42 K. Peng, J. Guo, H. Chen, M. Xie, X. Zhang, X. Huang, G. Xing, L. Shao and C. Qi, Copper Phthalocyanine Functionalized Polystyrene Superfine Fibers for the Photodegradation of Methyl Orange, *Fibers Polym.*, 2023, **24**, 3799–3808.
43 T. Mirmajidi, F. Chogan, A. H. Rezayan and A. M. Sharifi, In vitro and in vivo evaluation of a nanofiber wound dressing loaded with melatonin, *Int. J. Pharm.*, 2021, **596**, 120213.
44 B.-D. Zheng, Z.-L. Huang, L.-L. Lv, W.-L. Lan, J.-Q. Hu, X. Li, B.-Y. Zheng, M.-R. Ke and J.-D. Huang, A pH-sensitive nanoagent self-assembled from a highly negatively-charged phthalocyanine with excellent biosafety for photothermal therapy, *J. Mater. Chem. B*, 2021, **9**, 2845–2853.
45 B.-D. Zheng, Z.-L. Huang, L.-L. Lv, W.-L. Lan, J.-Q. Hu, X. Li, B.-Y. Zheng, M.-R. Ke and J.-D. J. Huang, A pH-sensitive nanoagent self-assembled from a highly negatively-charged phthalocyanine with excellent biosafety for photothermal therapy, *J. Mater. Chem. B*, 2021, **9**, 2845–2853.
46 J. E. Cruse-Sawyer, J Griffiths, B. Dixon and S. B. Brown, The Photodynamic response of two rodent tumour models to four zinc (II)-substituted phthalocyanines, *Br. J. Cancer*, 1998, **77**, 965–972.
47 B.-D. Zheng, J. Ye, Y.-Y. Huang and M.-T. Xiao, Phthalocyanine-based photoacoustic contrast agents for imaging and theranostics, *Biomater. Sci.*, 2021, **9**, 7811–7825.
48 B. Henderson, B. Owczarczak, J. Sweeney and T. Gessner, Effects of photodynamic treatment of platelets or endothelial cells in vitro on platelet aggregation, *Photochem. Photobiol.*, 1992, **56**, 513–521.
49 L. Mei, Z. Xu, Z. Miao, M. Yun, Y. Luan, D. Yang and L. Xia, Polymyxin B-functionalized phthalocyanine for chemo-photodynamic antibacterial therapy in enhanced wound healing, *New J. Chem.*, 2021, **45**, 6450–6457.
50 N. Malanovic and K. Lohner, Gram-positive bacterial cell envelopes: The impact on the activity of antimicrobial peptides, *Biochim. Biophys. Acta*, 2016, **1858**, 936–946.
51 E. Baigorria, J. E. Durantini, M. A. Di Palma, N. S. Gsponer, M. E. Milanesio and E. N. Durantini, Amphiphilic tricationic Zn(II)phthalocyanine provides effective photodynamic action to eradicate broad-spectrum microorganisms, *Photochem. Photobiol. Sci.*, 2021, **20**, 939–953.